Ligand-Bound Quantum Dot Probes for Studying the Molecular Scale Dynamics of Receptor Endocytic Trafficking in Live Cells

Sujata Sundara Rajan,[†] Hong Yan Liu,[†] and Tania Q. Vu[†,‡,*]

[†]Department of Biomedical Engineering and [‡]Neuroscience Graduate Program, Oregon Health & Science University, 3303 SW Bond Avenue, 13B, Portland, Oregon 97239

ABSTRACT Endocytic receptor trafficking is a complex, dynamic process underlying fundamental cell function. An integrated understanding of endocytosis at the level of single or small numbers of ligand bound-receptor complexes inside live cells is currently hampered by technical limitations. Here, we develop and test ligand nerve growth factor-bound quantum dot (NGF-QD) bioconjugates for imaging discrete receptor endocytic events inside live NGF-responsive PC12 cells. Using single particle tracking, QD hybrid gel coimmunoprecipitation, and immunocolocalization, we illustrate and validate the use of QD-receptor complexes for imaging receptor trafficking at synchronized time points after QD-ligand−receptor binding and internalization ($t = 15-150$ min). The unique value of these probes is illustrated by new dynamic observations: (1) that endocytosis proceeds at strikingly regulated fashion, and (2) that diffusive and active forms of transport inside cells are rapid and efficient. QDs are powerful intracellular probes that can provide biologists with new capabilities and fresh insight for studying endocytic receptor signaling events, in real time, and at the resolution of single or small numbers of receptors in live cells.

KEYWORDS: endocytosis · quantum dot · trafficking · neurotrophin · receptor · microtubule · active transport

Endocytic trafficking of membrane surface-expressed receptor proteins is a complex and dynamic process that is critical to governing cellular signaling and consequent cell function. Endocytic regulation of surface-expressed receptor proteins involves receptor internalization, transport, and breakdown in a series of intracellular vesicle containers in a crowded cytoplasmic environment.[1−4] Understanding receptor endocytic trafficking at the level of single or small numbers of receptors, at specific time points during a receptor's lifetime, has been a challenge in biology. Current bioimaging and biochemical methodologies face limitations which make difficult the dynamic detection of discrete ligand−receptor complexes and probing of their associated proteins. First, the fluorescent dyes and genetically engineered protein tags (Cy3, GFP) are dim, and their receptor labeling produces diffuse fluorescence, thus preventing prolonged glimpses of discrete groups of receptor molecules for substantial lengths of time. Second, GFP-tagged receptors are expressed in random amounts inside cells and therefore the state in a lifetime of any particular tagged-receptor protein is unknown. Third, it is impossible to distinguish ligand-bound *versus* free GFP-tagged receptors from one another. Fourth, determination of the association of receptors with other protein/vesicle compartments cannot be easily correlated with receptor dynamics since both real time imaging and biochemical assays are performed separately and because the sensitivity limitations are often done under different experimental conditions, making data difficult to interpret. A sensitive probe that would allow investigators to obtain dynamic information about the real time movement of single or small numbers of receptors, and identify *in vivo* receptor interactions with other cellular protein (*e.g.*, vesicle, ligand) and the vesicle containers in which receptors are transported at known time points during a receptor's lifetime would be of great value to investigators.

Quantum dots (QDs) are fluorescent nanoparticles that may offer solutions to the current technical limitations encountered in studying receptor dynamics inside cells. QDs are intensely bright, allowing the detection and resolution of single fluorescent particles, and their photostability exceeds that of fluorescent-dye-tagged proteins.[5−10] Furthermore, QDs can be introduced, in a synchronized and controlled manner, to cells in order to selectively bind receptors. While the value of QDs as tags for activating and tracking proteins on the extracellular membrane surface has been

Ⓦ This paper contains enhanced objects available on the Internet at http://pubs.acs.org/journals/ancac3.

*Address correspondence to tvu@bme.ogi.edu.

Received for review December 3, 2007 and accepted April 15, 2008.

Published online May 20, 2008.
10.1021/nn700399e CCC: $40.75

well-demonstrated,[11–21] and the capability of cells to internalize QDs into endocytic vesicles is well-recognized,[6,13,22–31] the potential use of QDs as intracellular tags for dissecting specific endocytic processes is not understood.

Here, we test the hypothesis that QDs can serve as physiologically faithful biological probes for tracking the endocytic regulation of single QD-receptor complexes inside live cells. We use QDs that are conjugated to the peptide growth hormone, nerve growth factor (QD-NGFs). NGF is a ligand that activates NGF receptors (TrkA and p75) and plays critical roles in regulating intracellular signaling in neurons.[32–36] We and others have recently demonstrated that QD-NGFs are capable of activating TrkA receptors,[37] that intact QD-NGF-TrkA complexes are internalized into cells, and that QD-NGFs can be visualized in dynamic movement in cells.[27,38,39] In the present studies, we show through a combination of single particle tracking, QD hybrid gel coimmunoprecipitation, and immunostaining assays, all of which can be implemented in the same experimental preparation, that QDs serve as intracellular probes for faithful tracking of receptor endocytosis at synchronized time points after their binding and internalization in live cells. The additional value of these probes is illustrated by the unique observations that (1) internalized receptors are processed with strikingly synchronized phases of endocytosis and that (2) both diffusive and active forms of transport are rapid and efficient despite the crowded cytosolic cellular environment. Application of these QD probes to understanding endocytic regulation at the scale of single or small numbers of receptor complexes will yield new insight into how intracellular endocytic mechanisms shape cellular signaling and govern overall cell function.

RESULTS AND DISCUSSION

Tracking Single QD-NGF-Receptor Complexes. In past work, we demonstrated that QD-NGFs retain bioactivity, bind to TrkA receptors, and activate TrkA signaling to induce neurite outgrowth.[27,37,40] Moreover, QD-NGF-TrkA complexes can be identified inside cells, and QD-NGF complexes can be visualized in motion inside cells.[27,37] Here, we first quantified the specificity of QD-NGF binding by counting the number of QDs that were bound when cells were treated with QD-NGFs compared to the number of QDs that were bound when cells were treated with control QD-streptavidin (the portion of the probe that does not contain the biotinylated NGF ligand). Following, we tested the possibility of using single particle tracking to observe the motion of QD-NGFs inside live cells.

Immediately following treatment (15 min of QD-NGF incubation at 37 °C), QD-NGFs bind to PC12 cell membranes in a punctate pattern (Figure 1A). In contrast, cells treated with control QD-streptavidin at the same concentration do not show a significant degree of fluorescent binding. At $t > 15$ minutes, a majority (~80−90%) of membrane-bound QD-NGFs are rapidly internalized into the cell cytosol. Figure 1B is a representative image showing that QD-NGFs have disappeared from the plane of the membrane and can be found at a *z*-plane that is 5 um from the top membrane surface, within the cytosol at 18 min after QD-NGF treatment. We know that a distance of $z = 5$ um from the top membrane surface is clearly located in the cell cytosol on the basis of three observations: (1) the NGF-treated PC12 cells used in this work consistently measure 8−10 um in cell diameter (measured from 0.5 um thick z-stacks across 15 cells, see Supporting Information, Figure S1), (2) from a focal imaging plane that is 5 um into the cell, we consistently measure a distance of several micrometers before reaching the collagen substrate-coated dish floor, and (3) a focal imaging plane of 5 um into the cell is never coincident with the sparse, uniformly dispersed QD-NGF populations which adheres to the collagen and marks the plane of focus at which the bottom membrane of the cell contacts the dish floor. These results show that time course of QD-NGF internalization is rapid and similar to that for known measures of NGF-activated TrkAs internalization in the PC12 cells. This contrasts the slower internalization rate of NGF-activated p75 receptors (internalization rate $t_{1/2}$=~42−50 min), suggesting that we are predominantly observing NGF-TrkA internalization at early time points.[41–45]

Because of difficulty distinguishing between NGF-binding to TrkA and p75 receptors, we use the term QD-NGF-TrkAs only in cases where this can be directly confirmed. Figure 1C shows quantitative measures of QD-NGF specific binding and illustrates that the likelihood of observing membrane-bound QD-NGFs *via* NGF-mediated interactions is ~93% (26 NGF-QDs: 2 streptavidin-QDs) and the likelihood of observing internalized QD-NGFs *via* specific NGF-mediated interactions is 91% (30 NGF-QDs/3 streptavidin-QDs). These data show that QD-NGFs bind to the cell membrane surface and are subsequently endocytosed into cells *via* the NGF working end of the QD-NGF probe.

Internalized QD-NGFs (at $t > 20$ min after treatment) were found to be composed of individual QD-NGFs as they all exhibited QD-NGF fluorescence fluctuations, or "blinking", and an anisotropic oval-shaped fluorescence profile characteristic of single ellipsoid 655 nm (red) QDs.[7] Figure 1D illustrates both of these features for a single QD-NGF tracked in the cell cytosol. The single particle tracking algorithms applied were successful in tracking the movement of single QD-NGF complexes inside cells and could successfully interpolate between frames during which QDs blinked (*e.g.*, the second and fourth frames in Figure 1D).

QD-NGF Dynamics Reflect Distinct, Uniformly-Regulated Stages of Endocytosis. Particle tracking of individual QD-NGF complexes revealed a variety of dynamics that could

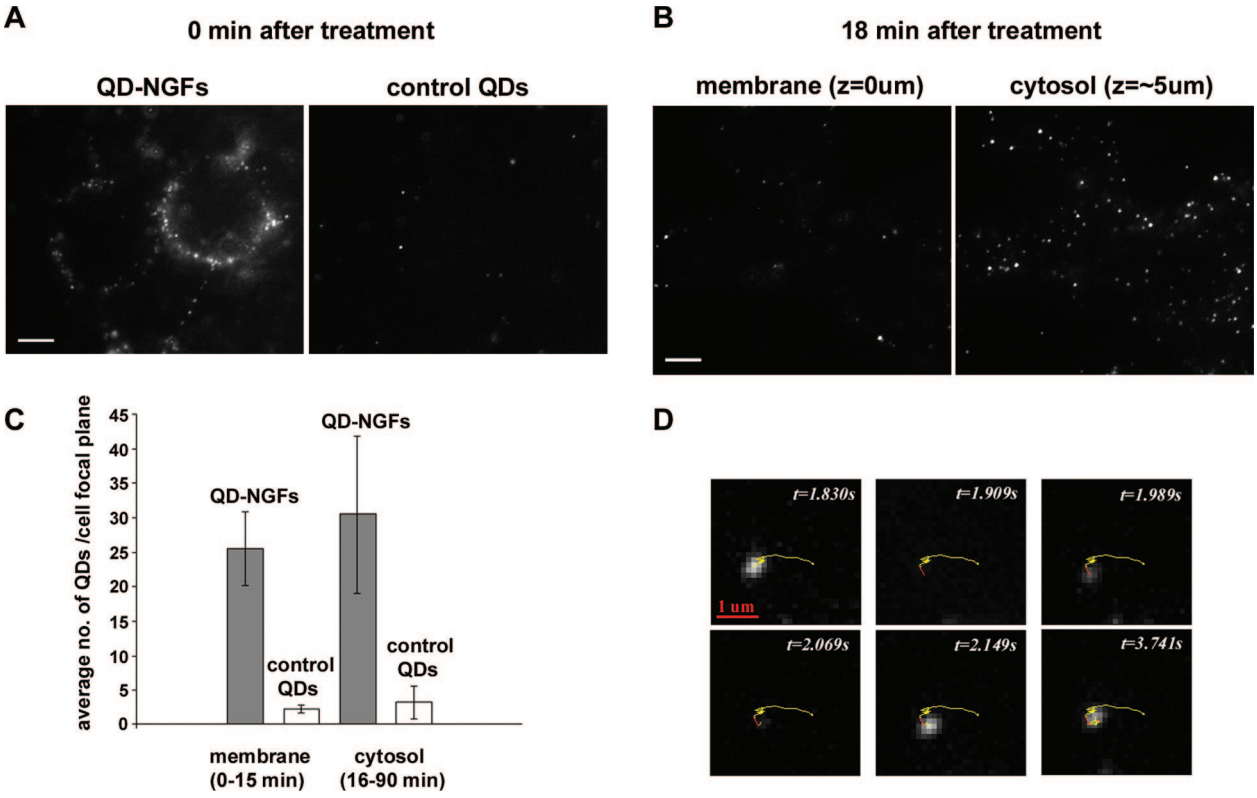

Figure 1. QD-NGF-receptor specific binding, rapid internalization, and single QD tracking in PC12 cells. (A) PC12 cells examined immediately after 10 nM QD-NGF treatment show punctate fluorescence at membrane surface at $t = 0$ after treatment (15 min preincubation with QD-NGF at 37 °C). Parallel control experiments using control 10 nM QD-streptavidin (the portion of the QD-NGF probe that does not contain the biotinylated NGF ligand) show a lack of significant fluorescence binding. Images were acquired and processed under the same conditions. (B) QD-NGF internalization at $t > 15$ min after treatment. At $t = 18$ min, punctate QD-NGF fluorescence disappears from the membrane surface (left image) and is found in the same field of view at a lower plane of focus in the cell (~5 μm from the cell membrane). Z-stack information shows that this focal imaging plane resides within the cell interior (see text and Supporting Information S1). (C) Histogram showing the number of QDs per cell focal plane for cells treated with QD-NGF and control QD-streptavidin. Likelihood of observing membrane-bound QD-NGFs *via* NGF-mediated interactions is ~93% (26 NGF-QDs/2 streptavidin-QDs), and the likelihood of observing internalized QD-NGFs *via* specific NGF-mediated interactions is 91% (30 NGF-QDs/3 streptavidin-QDs). Focal planes are located at the cell membrane surface and cell center (~5 μm from the membrane surface). QD counts taken at $t = 0-15$ min and $t = 16-90$ min after treatment from a total of 90 cells (3 independent experiments: control membrane $n = 21$ cells; control cytosol $n = 28$ cells; test membrane $n = 12$ cells; test cytosol: $n = 29$ cells). Error bars are std. (D) Particle tracking of an internalized single QD-NGF complex. Single QD-NGF composition is indicated by QD-NGF fluorescence blinking fluctuations and an anisotropic ellipsoid fluorescence profile. Particle tracking algorithms successfully track QD-NGF movement and can interpolate between frames during QD blinking (*e.g.*, the second and fourth frames).

be grouped into four general classes of movement. These general classes of movement occurred at distinct time intervals after endocytosis. First, immediately following QD-NGF treatment, QD-NGF complexes exhibited diffusive movement that circumscribed the membrane surface. This was most evident at $t = 15$ min, when most QD-NGF complexes had moved from the membrane surface into the cytosol, and the motion of QD-NGF complexes remaining on the membrane could be followed at durations of 20–30 s with confidence that the same, single QD-NGF complex was tracked (Figure 2A). Second, after internalization, QD-NGF complexes experienced two general forms of cytosolic diffusion: (a) restricted diffusion, which consisted of loosely confined random displacements (Figure 2A, white arrowheads) and (b) unrestricted diffusion (Figure 2A, white arrows) which traversed a large area and did not appear to retrace its path. We defined all trajectories that had a steady baseline and were composed of small fluctuations, ($< \pm 200$ nm), interspersed with large, intermittent (>200 nm) fluctuations, as exhibiting restricted diffusion (Figure 5A). We defined all trajectories that had no steady baseline (average baseline $> \pm 200$ nm) as exhibiting unrestricted diffusion (Figure 5D). Mean square displacement analysis of both of these types of fluctuations indicated that they were diffusive (data not shown). Third, many QD-NGF complexes exhibited active transport as evident by linear, directed movements (Figure 2A). These directed movements exhibited sustained transport in a single direction and, in some cases, sustained transport in a forward and backward direction. We defined all trajectories that contained at least one net linear, saltatory displacement (Figure 6A) as exhibiting active transport. Fourth, at longer durations ($t > 60$ min), QD-NGF complexes exhibited confined diffusion, that consisted of diffusive fluctuations which were similar to the baseline fluctuations observed with restricted diffusion; however, these

A

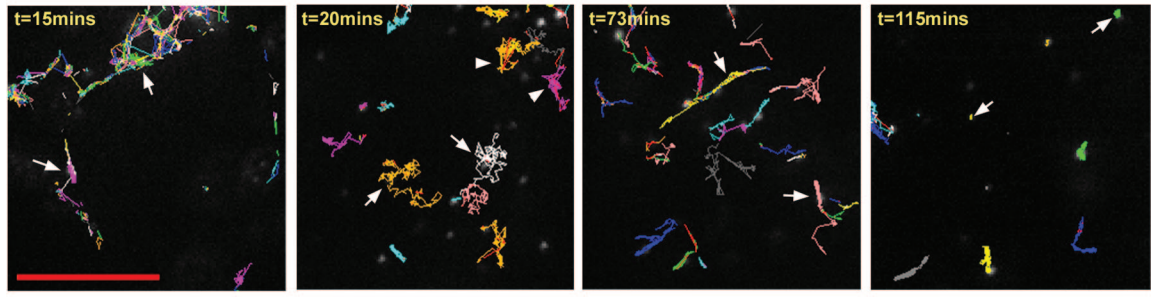

B

Time after NGF-QD treatment	Cytosolic diffusion	Active transport	Confined diffusion
0-15 min	—	—	—
16-30 min	24 ✲	6	1
31-60 min	30 ✲	16 ✲	1
61-90 min	19	14 ✲	9 ✲
91-150 min	15	7	31 ✲

Figure 2. QD-NGF complexes exhibit distinct dynamics at progressive phases of endocytic trafficking. (A) Trajectories of QD-NGF complexes at progressive time points that are superimposed on corresponding video stills show synchronized phases of movement: (1) membrane diffusion; (2) two forms of cytosolic diffusion: "restricted diffusion" (arrowheads) and "unrestricted diffusion" (arrows); (3) active transport; and (4) confined diffusion. Scale bar = 5 μm. (B) Table showing of the number of trajectories categorized by type of movement at each time interval. Trajectories were categorized without prior knowledge of their time point (see text for criteria). A total of 181 QD-NGF trajectories of 20–30 s duration each were examined from 3 independent experiments consisting of 2 dishes each. Asterisks mark onset of distinct stages of dynamic movement that reflect phases of passage through endocytic pathways.

trajectories were confined to movement that within spherical regions (Figure 2A). Trajectories that were defined by a steady baseline $< \pm 200$ nm (Figure 7A) and whose trajectories were spherical were defined as exhibiting confined diffusion.

To determine if these general classes of movement were associated with distinct phases of endocytosis, we randomly tracked a large set of individual QD-NGF complexes inside cells ($n = 181$) and then categorized the motion of each QD-NGF complex without prior knowledge of the time point at which the data were obtained. The table in Figure 2B shows a cumulative summary that indicates that QD-NGF complexes exhibit movements synchronized to distinct endocytic phases. First, QD-NGF complexes undergo restricted and unrestricted diffusion ($t = 16-30$ min). Following this, QD-NGF complexes undergo active transport ($t = 30-90$ min). Finally, QD-NGFs undergo confined diffusion ($t = 90-150$ min). At $t = 90-150$ min, a subpopulation of QD-NGFs exhibit diffusive-based dynamics of confined movement. Given the slower time course of NGF-p75 internalization compared to that of NGF-TrkA, this subpopulation could represent QD-NGF-p75 receptor complexes that are internalized at later time points.[44,45] Alternatively, this subpopulation could also represent QD-NGFs that remain in cytosolic diffusion for longer time periods.

These data show that QD-NGF complexes undergoing endocytic trafficking inside cells exhibit distinct types of movement that reflect underlying phases of endocytosis. A valuable trait of these QD-NGF probes is the capability to monitor the single experience of a large population of QD-NGF complexes. This allowed us to make the new observation that QD-NGF complexes, once endocytosed, do not exhibit much variation; rather endocytic processing occurs in phases that are regulated with a high degree of uniformity.

QD Hybrid Gel Co-Immunoprecipitation Assays Confirm Intact QD-NGF Probe-Receptor Composition. NGF ligands remain associated with their receptors inside cells for prolonged periods of time after endocytosis,[35,45–52] but may eventually dissociate from receptors in progressively acidic late vesicles. To confirm that QD-NGFs remain associated with NGF receptors after their internalization and at progressive time points during endocytosis, we use a novel QD hybrid gel coimmunoprecipitation technique.[40] An important advantage of this method compared to traditional assays (immunoprecipitation, surface biotinylation) is that we can discriminate surface-derived QD-NGF-activated TrkAs from other surface-expressed or cytosolic TrkAs. Moreover, QD bright fluorescence allows extremely sensitive detection, and therefore low concentrations of QD-NGF can be used which are comparable to the experimental conditions in which QD-NGF dynamic tracking experiments are performed.

The color image in Figure 3A is an electroblot of cell lysates collected at fixed time points from live PC12 cells treated with QD-NGFs. The control lane is loaded with a sample of freely soluble QD-NGF (*e.g.*, no cell ly-

sate). QD-NGF complexes fractionate in a defined band, and steady levels of QD-NGFs are present in cell lysates at all time points $t = 0-150$ min following QD-NGF treatment. Cell lysate-collected QD-NGF collected from cell-lysates (lanes $t = 0-150$ min) migrate more slowly through the gel compared to freely soluble (control) QD-NGFs, and indicate that cell lysate-collected QD-NGFs may be complexed to NGF receptors such as TrkA. Figure 3B shows the same membrane after hybridization with anti-TrkA-green QDs, and shows a hue change in the bands in all lanes (lanes $t = 0-150$ min but not control lane) indicating that QD-NGF-TrkA complexes are present. Little change was seen in the levels of QD-NGF-TrkA complexes for time points up to 2.5 h after treatment. This is again more clearly illustrated in the grayscale images that separate the color image into monochrome RGB separated channels (blue channel contains no information, and is not shown). Again, a lack of green fluorescence in the control soluble QD-NGF lane confirms that the green fluorescence is due to specific binding of red QD-NGF-TrkA-green QDs. Additional negative control experiments performed under the same experimental conditions as that used in Figure 3 further verify that anti-TrkA green QDs did not produce nonspecific binding to TrkA complexes or QD655-streptavidin alone (see Supporting Information, Figure S2).

In summary, these data illustrate a method for confirming that endocytosed QD-NGF-TrkA receptors remain intact inside cells. We find a sustained persistence of QD-NGF binding to surface-derived TrkA which is consistent with past biological studies using free NGF (>50% of surface biotinylated TrkA is intact in cells at 60−100 min after internalization).[43,45] This supports the physiological-relevant behavior of QD-NGF probes for tracking receptor endocytosis.

QD Immuno-Colocalization Provides Identity of QD-NGF Vesicles for Correlation with QD-NGF Dynamics. Upon internalization into clathrin-coated pits, NGF-receptors (TrkA and p75) are subsequently transferred into early endosomes.[45,53] To identify the compartments in which QD-NGF complexes may reside during early endocytosis and to relate this to the QD-NGF dynamics we observed, we performed colocalization studies of QD-NGF complexes with early endosome antigen-1 (EEA-1), a marker for early endosomes.[54]

Immuno-colocalization experiments were performed with QD-NGF-treated PC12 cells under conditions identical to live cell tracking experiments. Cells were fixed at a series of time points, immunostained and imaged. Measurements of radioactive NGF in PC12 cells show little difference in NGF binding and internalization kinetics of at 10−40 nM.[55] Therefore, QD-NGF concentrations were titrated (10−40 nM), and an optimal concentration of 40 nM (4× the concentrations used in live cell experiments) was found to yield a number of internalized QD-NGF-receptor complexes optimal for detecting changes in colocalized QD populations. Figure 4A shows projection images of cells fixed at $t = 15$, 30, and 45 min. Because the size of QD-NGFs and the vesicles that contain them are less than that of an optical section thickness (0.5 um), the fluorescence of QD-NGF complexes and vesicle endosomes was usually confined to a single optical section; this combined with the bright emission intensity of QDs allowed punctate and distinct colocalization of QD-NGFs within immunostained vesicle compartments. At $t = 15$ min, several red QD-NGF-receptor puncta colocalize with green EEA-1 early endosomes (Figure 4A), and examination of zoomed-in images of colocalized puncta showed clear containment of QDs inside early endosomes (Figure 4D). At $t = 30$ min, a greater number of QD-NGF-receptor complexes have moved away from the membrane periphery and further toward the cell center, evidenced by the clear presence of fluorescence-free dark round nuclei. At this phase of endocytosis, QD-NGF-receptor complexes can be found in early endosomes (Figure 4B,E). However, at $t = 45$ min, there is little colocalization of QD-NGF-receptors with EEA-1 early endosomes (Figure 4C,F).

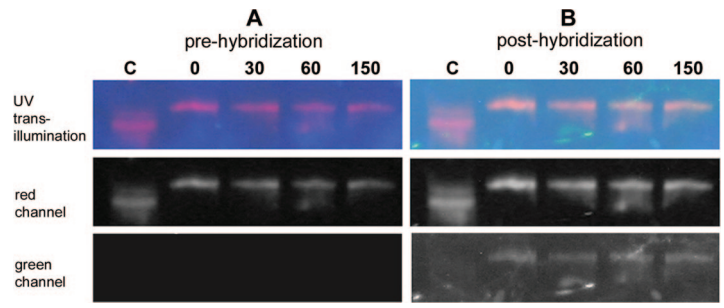

Figure 3. QD hybrid gel coimmunoprecipitation directly confirms QD-NGF binding to TrkA receptors at progressive endocytic phases. Color images are electroblots of fractionated (red) QD-NGFs obtained from cellular lysates prior to hybridization (A) and posthybridization with (green)-QD anti-TrkA receptor antibody (B). Lanes are $t = 0$, 30, 60, 150 min after QD-NGF treatment and a control lane containing soluble QD-NGFs (no cell lysates). Color images were viewed under UV trans-illumination and monochrome images below are red and green separated channels. Respective color and channel-separated images in panels A and B were obtained and processed under the same imaging conditions. The increased background brightness after posthybridization (B) is caused by transparency-enhanced membrane wetting and the presence of posthybridization-applied blocking proteins.

These data are consistent with expected receptor endocytic trafficking and show that QD-NGF complexes transiently reside in early endosomes in early phases of endocytosis. The time period in which the bulk of QD-NGF-receptor complexes colocalize with early endosomes ($t < 45$ min) occurs before the time period during which we observe the bulk of QD-NGF-receptor microtubule-driven transport ($t = 30-90$ min) (Figure 2B, table). This is in line with previous work showing that NGF-TrkA complexes are sorted from early endosomes into MVB/late endosomes,[45] and that sorting into early endosomes occurs before long-distance transport in late endosomes.[36,56]

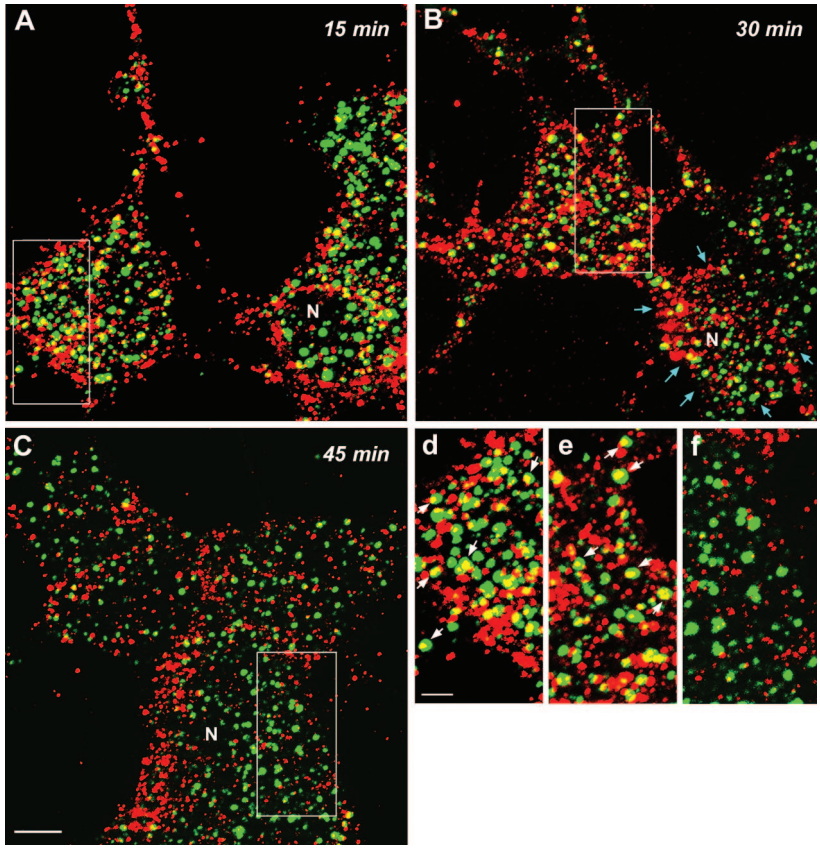

Figure 4. Imuuno-colocalization assays identify specific QD-NGF vesicle compartments for correlation with QD-NGF dynamic behavior. Panels A, B, and C show transient localization of QD-NGF in early endosomes. Collapsed vertical sections of PC12 cells treated with 40 nM QD-NGFs (red) and immunostained with the early endosomal marker anti-EEA-1-Alexa 488 (green) at $t = 15$, 30, and 45 min after QD-NGF treatment. Yellow puncta denote colocalization of QD-NGF complexes with early endosomes. Blue arrows outline approximate location of cell membranes (corresponding to DIC bright field images at middle of the *z*-stack) and "N" denotes cell nuclei. Scale bar: 5 μm. (d, e, f) Magnified sections are indicated respectively by the boxed region in panels A−C and shows a pattern of QD-NGF colocalization with EEA1 positive endosomes which predominates at $t = 15$ and 30 min (arrows), but which disappears at $t = 45$ min. Note: QD-NGF and EEA-1 vesicle fluorescence predominantly localize in single vertical sections (0.5 μm thickness). Scale bar: 2 μm.

QD-NGFs Show Receptor Diffusion in Cells is Elastic and Far-Ranging. QD-NGFs exhibited diffusive behavior which was consistent with past observations of ligand-bound receptors and vesicle endosomes undergoing early endocytic diffusive dynamics, prior to active transport.[57,58] We applied QD-NGF dynamic tracking to study this diffusive behavior. Quantitative analysis indicated that QD-NGFs exhibited restricted diffusion (79% of all QD-NGF complexes undergoing cytosolic diffusion) compared to unrestricted diffusion. Restricted diffusion was characterized by a steady baseline that contained both a large and a small component of fluctuation (Figure 5A, video **1**). Both small and large fluctuations were reversible, straying away and then returning to the same baseline. The elastic nature of these movements suggest that they involve collisions of the QD-NGF complex and the vesicle endosome it resides in with other deformable cytosolic structures. Large fluctuations were as large as 1 μm; this is an appreciable distance compared to the diameter of a cell (1/10 diameter of a cell) (Figure 5B). These large displacements thus likely represent the collision of an endosome containing QD-NGF-complexes with other cytosolic structures, such as cytoskeletal filaments, which are known to possess elastic properties.[2] Small fluctuations exhibited an average deviation from a baseline of ± 122 nm, and 95% of all fluctuations were <250 nm (Figure 5C). These small displacements could represent smaller scale collisions of QD-NGF vesicle endosomes with other elastic cytosolic structures as well as collisions of the QD-NGF complex within vesicle endosomes (early endosomes, late endosomes, and lysosomes measure ~250 nm in PC12 cells[59]).

A minority of QD-NGF complexes undergoing cytosolic diffusion, 21% (15/73 cases of cytosolic diffusion) experienced unrestricted diffusion that was less constrained (Figure 5D and video 2). This form of unrestricted diffusion was composed of a mixture of different types of displacements, including large and small fluctuations, sustained pauses, and a lack of a steady baseline (Figure 5D). These QD-NGF complexes were not undergoing true "unrestricted diffusion" given the crowded cytosolic environment and traversed appreciably large regional diameters (2.5−6 μm). The presence of sustained linear trajectories indicated that unrestricted diffusive transport could involve transitory interactions with microtubule networks (linear movement, Figure 4D). Because of difficulty in obtaining a large sample of these fewer-occurring numbers of QD-NGF complexes undergoing unrestricted diffusion, we did not further analyze the dynamics of unrestricted diffusive motion.

In summary, QD-NGF complexes exhibit diffusive dynamics that are consistent with past studies.[57,58] A majority of QD-NGF complexes undergo restricted diffusive movements that are elastic and likely involve the collision of the QD-NGF complex within endosome and other deformable cytosolic structures. The new observation that QD-NGF complexes undergo far-ranging, elastic fluctuations (at appreciable distances of up to 1/10 the diameter of a cell), questions the conventional belief, based on mathematical modeling, that diffusion may be inefficient in the crowded cytosolic environment.[35,60]

QD-NGFs Show Uniform and Far-Ranging Receptor Transport on Single Microtubules. Active transport of receptors and other protein cargo inside cells is mediated through energy-expending molecular steps along cytoskeletal motor filaments, such as actin, and microtubules.[61,62] QD-

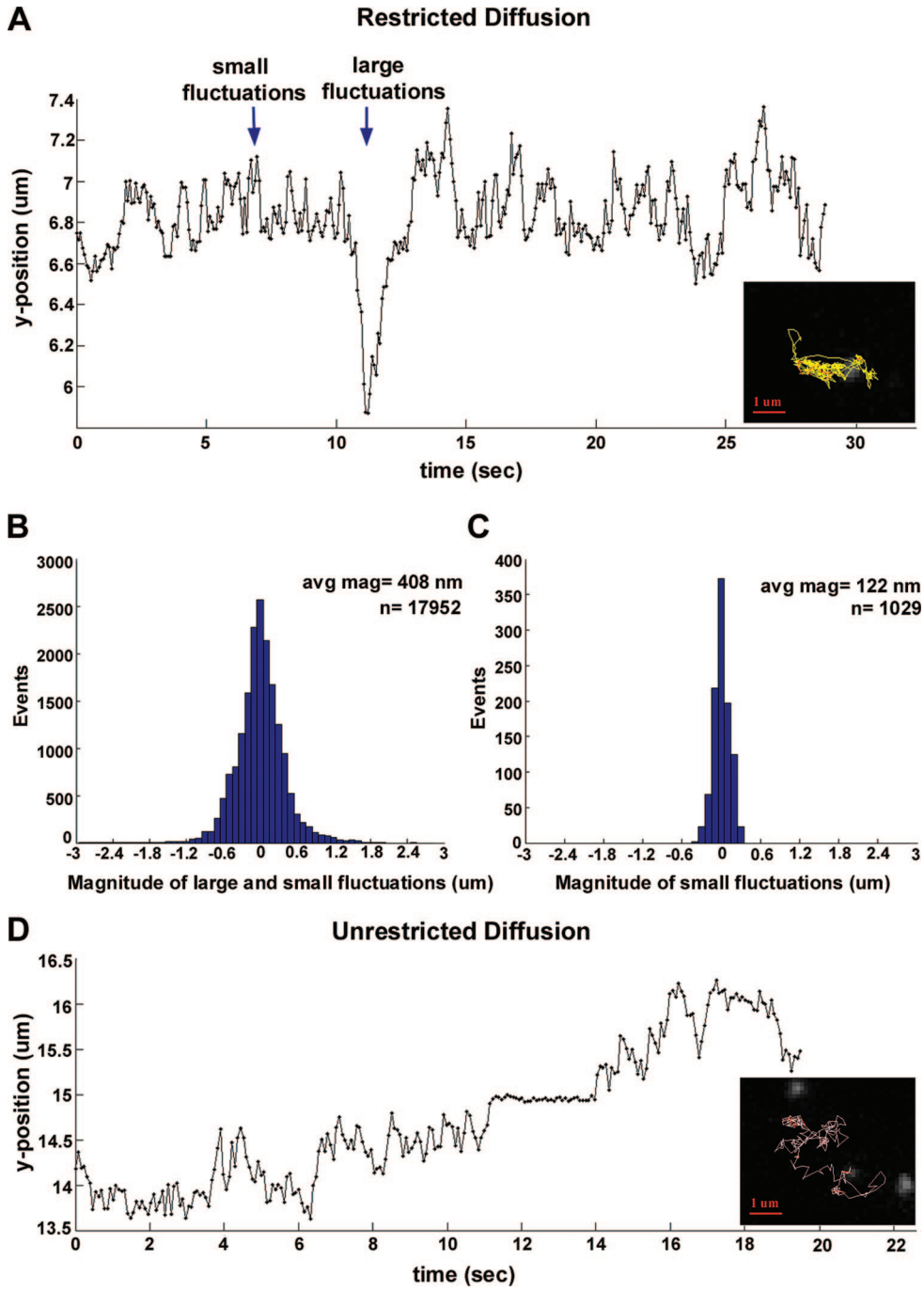

Figure 5. QD-NGF cytosolic diffusion is characteristic of early endocytosis but shows surprising far-ranging mobility. (A) Representative plot of QD-NGF complexes undergoing restricted diffusion. Movements consist of large and small components of fluctuations that are elastic, returning to a steady baseline. Inset is the corresponding trajectory of this QD-NGF complex (30 s duration, tracked at $t = 18$ min after QD-NGF treatment) (see video 1 for corresponding real time movie). (B) Histogram of the magnitude of all collected trajectories showing restricted diffusion. The average magnitude of restricted diffusion is ± 408 nm. Large fluctuations deviate in magnitude that are as large as 1 um from the baseline, a substantial distance relative to the size of a cell. All trajectories have been zeroed by subtracting the average position of a trajectory from all positions within a trajectory; *n* is the number of frames from sampled positions. (C) Histogram of magnitude of small fluctuations shows that the average size of small fluctuations was ±122 nm (95% of all fluctuations were <250 nm). Histogram constructed from positional plots selected by eye which did not contain large fluctuations. All trajectories have been zeroed by subtracting the average position of a trajectory from all positions within a trajectory; *n* is the number of frames from sampled positions. (D) Representative positional plot of QD-NGF complexes undergoing "unrestricted" diffusion shows a lack of steady baseline, a wide variety of positional displacements (large, small, pauses) and wide regional diameters that are covered (2.5−6 μm). Inset is corresponding trajectory of this QD-NGF complex (20 s duration, 20 min after QD-NGF treatment) (see video 2 for corresponding real-time movie).

Ⓦ An avi movie, video 1 , showing QD-NGF complexes undergoing restricted diffusion is available.

Ⓦ An avi movie, video 2 , showing QD-NGF complexes undergoing "unrestricted" diffusion is available.

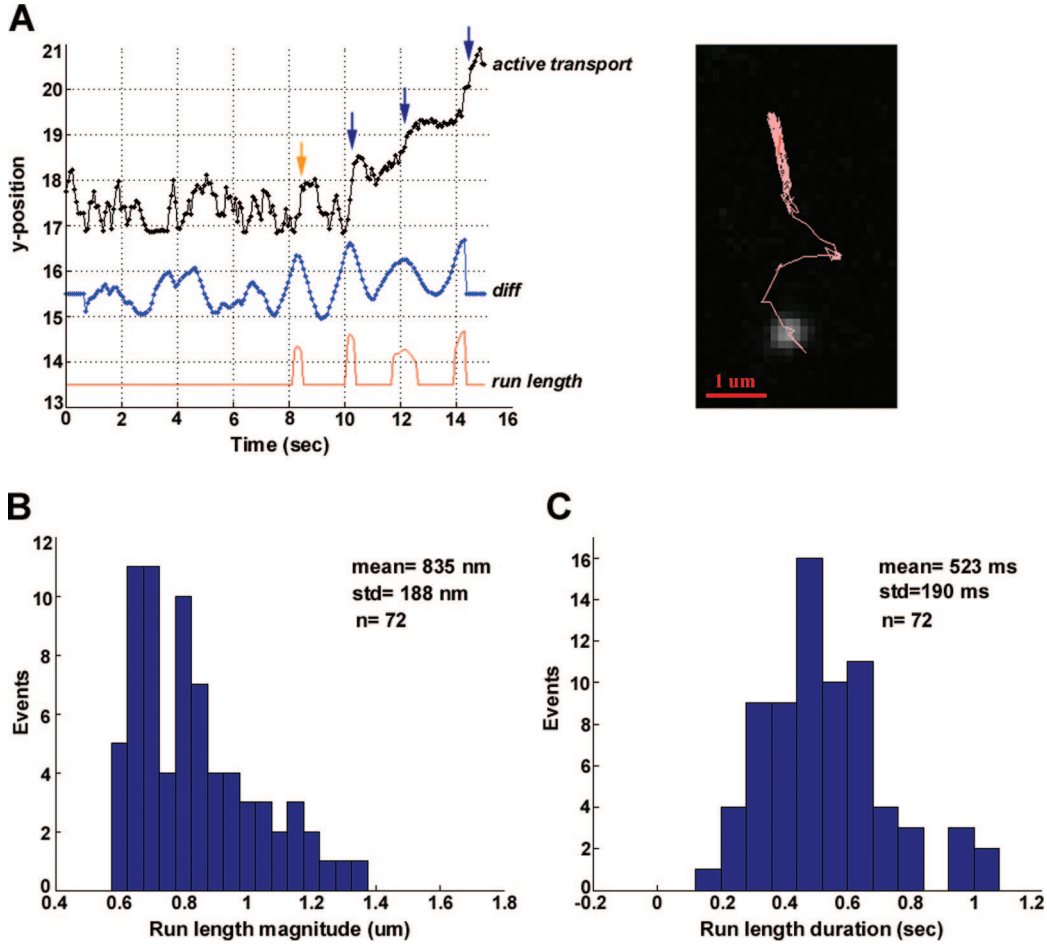

Figure 6. ***In vivo*** **active transport of QD-NGF complexes along single microtubule-motor run lengths is uniform and far-ranging. (A) Representative position plot of a QD-NGF complex showing active transport. Blue and red traces are the outputs of the automatic detection filters applied, *diff* and *run length*. Dark blue arrows indicate examples of a succession of single run lengths. Orange arrow depicts an example of diffusive fluctuations that can be mistakenly detected by the filter; these "false positives" were confirmed as infrequent (only 4 of a total of 72 run lengths were false, see Methods). Inset is the corresponding trajectory of this QD-NGF (15 s duration, tracked at $t = 73$ min after QD-NGF treatment) (see video 3 for corresponding real-time movie). (B) Histogram showing that the average run length traveled by QD-NGF-receptor complexes is 0.835 ± 0.188 μm (23% of the mean); 71% of total run lengths are within the range of 0.625−0.975 μm. ($n = 72$). (C) Histogram showing that the average duration of a run length is 0.52 ± 0.19 s (37% of the mean) ($n = 72$).**

Ⓦ An avi movie, video 3 , showing a QD-NGF complex demonstrating active transport is available.

NGF complexes exhibited active transport in the form of linear and directed displacements (Figure 6A, blue arrows; also video 3) that is consistent with that observed for microtubule transport.[63–65] These linear displacements represent a run length, or distance along, that protein cargo is transported before it detaches from the microtubule.[63,66] Run lengths occurred as single events interspersed among diffusive fluctuations, as a succession of run length events in one direction or as a succession of run lengths in a back and forth direction. The addition of 20 μM nocodazole, a microtubule depolymerizing agent, completely abolished these linear movements within 15−20 min, indicating that the principal mode of active transport was microtubule mediated. We measured the run-length distance and duration in order to characterize the dynamics of this microtubule-driven NGF-receptor transport.

Visual inspection of a total of 72 QD-NGF run lengths indicated that run lengths were distinct from diffusive fluctuations and stereotypical in shape. We verified this by applying a series of moving average filters to automatically detect and measure the distance and duration of run lengths (see Methods). The average run length traveled is 0.835 ± 0.188 μm (Figure 6B). Run length durations measured on average 0.52 ± 0.19 s and thus were also quite uniform (Figure 6C). The average speed of QD-NGF active transport was 1.6 μm/sec (ratio of average distance and duration). This speed is consistent with *in vitro* and *in vivo* speeds of measurements of net NGF and Trk receptor transport (0.2−2 μm/sec) on microtubule cytoskeletal filaments.[48–50,67]

The ability to visualize *in vivo* single QD-NGF complexes undergoing active transport revealed that receptor complexes undergo uniform and far-ranging transport

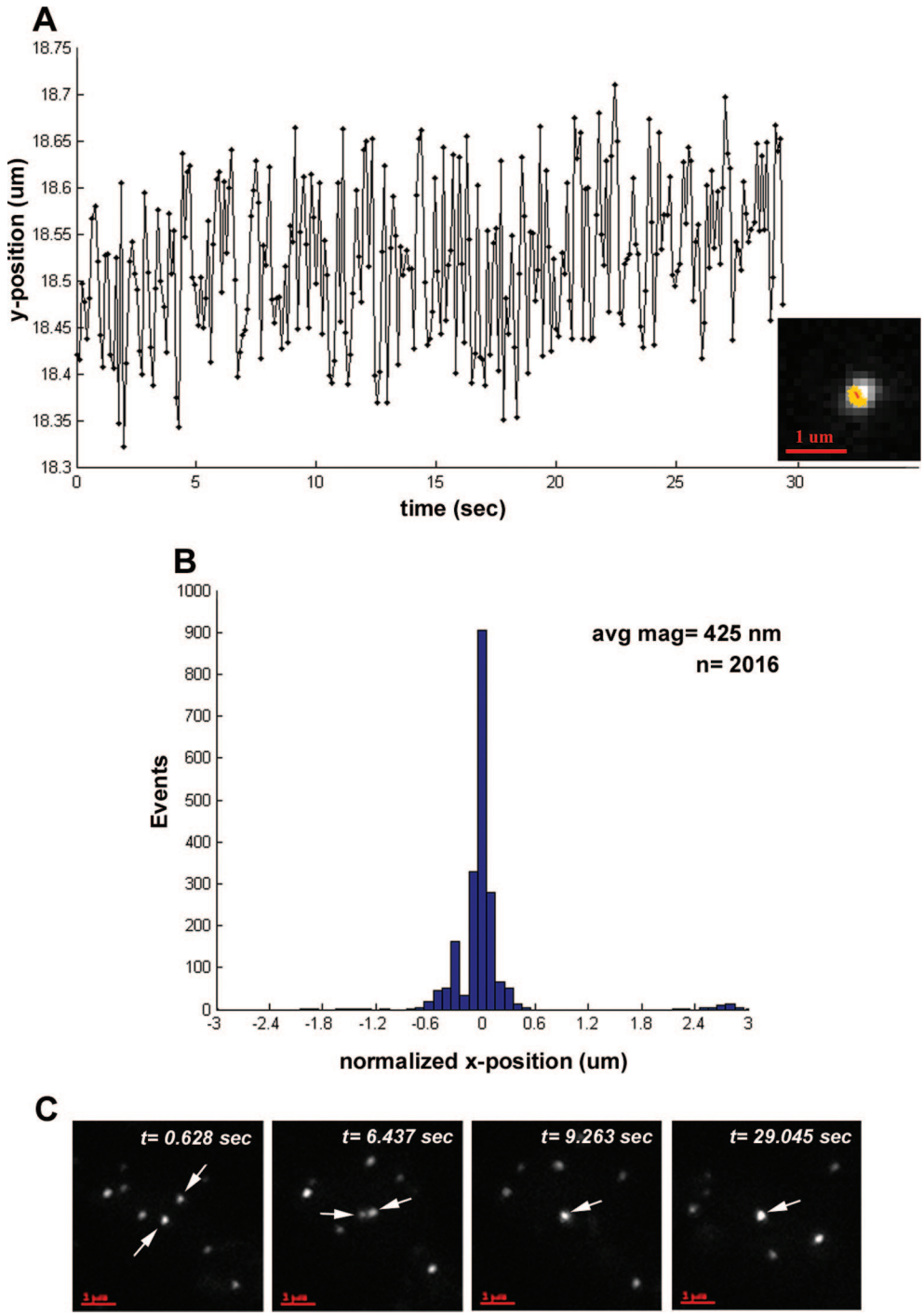

Figure 7. QD-NGF complexes fuse and experience spherically confined diffusion within late endosomes. (A) Representative positional plot of QD-NGF illustrating magnitude of confinement. Inset is the corresponding QD-NGF trajectory (30 s duration, tracked at t = 79 min after QD-NGF treatment) (see video 4 for corresponding real-time movie). (B) Histogram of the magnitude of all collected trajectories showing confined diffusion. The average magnitude of confined diffusion is ±425 nm and 80% of all excursions had a magnitude of ±250 nm. (C) Frames from a time-lapse video illustrating the fusion of two separate QD-NGF complexes (30 s duration, tracked at t = 73 min after QD-NGF treatment). Note the increase in QD intensity following combination (frames 3 and 4) (see video 5 for corresponding real-time movie).

Ⓦ An avi movie, video 4, illustrating magnitude of confinement is available.

Ⓦ An avi movie, video 5, illustrating the fusion of two separate QD-NGF complexes is available.

on microtubule filaments. This transport is very efficient; once a QD-NGF complex has bound to a microtubule filament, it is transported a distance of 1 μm (~1/10 cell diameter) along a microtubule before it disengages.

Real-Time Fusion of Vesicles Carrying QD-NGF Complexes in Late Endocytosis. We observed QD-NGF behavior that was consistent with endocytic trafficking in later stages of endocytosis. QD-NGF complexes moved in small dif-

fusive displacements that had an average magnitude of ±425 nm (80% of all excursions within 250 μm) in late endocytosis ($t > 90$ min). These displacements were similar to the small diffusive fluctuations observed at early phases of endocytosis (Figure 7A and video 4). However, diffusive movements found in early endocytosis, QD-NGF displacements were confined to distinct spherical-shaped regions (Figure 7A inset, video 4). QD fluorescence appeared larger and brighter at these later phases of endocytosis, suggesting that multiple QD-NGF complexes reside in these spherical compartments. In four instances, we observed the real-time fusion of two single (blinking) QD-NGF complexes which remained fused (Figure 7C, video 5). These data show that after active transport, QD-NGF dynamic behavior is consistent with behavior expected at late phases of endocytosis: QD-NGF complexes fuse into common late endosomal compartments and undergo spherically confined diffusion within these late compartments.

SUMMARY AND CONCLUSIONS

In this paper, we have used NGF ligand QD bioconjugate probes to investigate the molecular-scale dynamics of NGF-receptor complexes undergoing endocytic trafficking. Live cell single QD tracking experiments performed in parallel with QD hybrid gel coimmunoprecipitation and immuno-colocalization assays indicate that QD-NGF probes can be used to visualize the real time behavior of NGF-bound receptor complexes with nanometer-scale resolution. The time course of these dynamics can be correlated with the composition of QD-NGF-receptors complexes as well as the identity of associated QD-NGF endosomal vesicles. These sensitive QD-NGF probes differ from previous measurements in that they directly measure the behavior of small quantities of surface-derived, NGF-bound receptors.

Current techniques for visualizing the dynamics of discrete proteins are limited in discriminating neurotrophin-bound receptor complexes from that of free receptors and visualizing neurotrophin-receptor complexes in discrete numbers. For example, GFP-labeled proteins cannot resolve single protein complexes that are distributed in diffuse quantities inside cells. In addition, GFP techniques cannot easily discriminate among the different states of a particular protein's lifetime (*e.g.*, a receptor that has just been internalized *versus* a receptor that has been synthesized). While GFP techniques are suitable for visualizing the movement of larger endosomes, photobleaching remains a limiting factor in detecting and high-resolution tracking for extended durations.

Our results support the notion that QDs can be used as a tag on a surface receptor to faithfully report intracellular trafficking. First, QD-NGF complexes follow both diffusive and active transport dynamics that resemble studies of endosomal movement observed with GFP-tagged endosomes, viral particles, synthetic polymer complexes, and other QD-encapsulated endosomes.[29,31,38,39,57,58,68–70] Second, QD-NGF dynamics follow a progression of movement that is consistent with classical models of endocytosis: early phase of diffusive-based transport in early endosomes, transfer to vesicle endosomes that undergo active microtubule motor-based movement, and fusion of multiple compartments into common late endosomes.[1,4,71] A possible concern of using QD probes is that their size is larger than that of other fluorescent dyes; however, it is noteworthy that, in nature, viral particles of comparable or larger size can successfully hijack endocytic processes in cells.[54,72,73] An advantage of using QD-ligand-bound probes such as QD-NGF to track intracellular receptor dynamics is that the behavior of a ligand-bound receptor can be quantitatively described with precise spatial resolution without concern of fluorescence bleaching or diffusion of dyes from endocytic compartments. Future work using QD-protein probes designed to bind to engineered receptor tags will be useful for comparing the behavior of ligand-bound *versus* free receptors in the same experimental preparation. In addition, because it is currently not possible to accurately synthesize and purify QD-probes with known valence, future development along these lines will provide probes for comparing monovalent *versus* multivalent receptor pools.

The intracellular routes and fate of cell-internalized nanoparticles is dependent on the physiology of the particular cell system studied as well as the physiochemical and size characteristics of the nanoparticle complex.[74–78] A distinct feature of the QD nanoparticle complexes that we have studied is that the QD-NGF complex activates and targets a specific receptor and thus may be expected to follow the endocytic route of that of NGF ligand-TrkA receptors. In the absence of QDs, NGF-receptor complexes are endocytosed through clathrin-coated endosomes, transferred into early endosomes, and remain intact for sustained periods of time in later endosomes prior to transfer to lysosomes.[41,46,47,52,53] Our studies show several lines of evidence that are consistent with the idea that QD-NGF-receptor complexes are processed in a manner that is similar to that of NGF-receptor complexes: (1) QD hybrid gel coimmunoprecipatation assays show that sustained levels of QD-NGF-TrkA complexes are observed at $t = 15-150$ min after endocytosis (Figure 3), (2) QD complexes colocalize with early endosomes, (3) QD-NGF complexes show almost no colocalization with lysosomal markers at time periods up to 150 min (unpublished data), and (4) QD complexes can be mobile, concentrating at growth cone tips in longer term culture ($t = 48$ hrs),[27] rather than concentrating in a perinuclear fashion about the nucleus. Although further studies will be needed to trace the exact vesicular pathway that QD-NGF complexes pass through after inter-

nalization, these initial lines of evidence indicate that ligand-bound QDs will be faithful probes for mapping specific intracellular receptor trafficking pathways in cells and correlating this to discrete receptor dynamics.

Our initial application of QD-NGF probes to study NGF receptor dynamic trafficking points to several lines of evidence indicating that NGF trafficking operates with a strikingly high degree of efficiency at the molecular-size scale. First, the magnitude of single QD-NGF undergoing diffusive displacements as well as transport along microtubules (measured as run lengths) exhibits little size variation (Figures 5 and 6). Second, single QD-NGF complexes undergo endocytosis in a uniform and highly synchronized fashion (Figure 2). Third, while momentary interactions of endosomes with microtubule networks may temporarily move endosomes significant distances during early phases of diffusion movement,[79,80] we observed that there exist elastic displacements that occur during diffusive phases of endosomal transport. These elastic displacements appear to transport endosomes over far-ranging distances, but bounce back to a steady baseline. While it is believed that endosomal movement is expected to be severely hampered in crowded cellular compartments,[35,60] there is a possibility that QD-NGF endosomal complexes may also travel across substantial distances in an elastic manner, perhaps giving complexes momentary access to other substantially distant cellular sites (Figure 5A). Finally, the *in vivo* single microtubule run-length distances we measure are appreciable in size (1 μm average run length = $\sim$1/10 cell body), and similar to that measured in *in vitro* assays,[81] indicating that a well-regulated efficiency of underlying active transport mechanisms is retained inside cells. Endocytosis is a complex process involving the transfer and transport of NGF-receptors among different vesicle endosomes in a crowded cytoplasmic environment.[1–4] Perhaps these examples of efficiency, which emerge at the level of single or small numbers of ligand−receptor complexes, endosomes, and microtubule filaments, constitute multiple adaptive solutions that cells use to successfully orchestrate the complex process of endocytic trafficking.

METHODS

QD-NGF Conjugation. QD-NGFs were made using previously published methods.[37] Briefly, NGF (β-NGF, 1156-NG/CF, R&D Systems) was biotinylated *via* carboxyl group substitution using biotin hydrazide (Sigma) and 1-ethyl-3-(3-dimethylaminopropoyl)-carbodiimide (EDAC, Sigma) at stoichiometric ratios that result in three or less biotins per NGF. QD-NGF complexes were formed by gentle vortexing and incubation of biotinylated βNGF with red 655 streptavidin-QDs (Invitrogen) at a 1:1 molar ratio (4 °C, 1 h). Prior to conjugation, QDs are monodispersed as characterized using AFM, TEM, and fluorescence blinking.[37,82,83] After bioconjugation, nanoparticle QD-NGF conjugates remained monodispersed as confirmed by detection of QD fluorescence blinking and QD anisotropic ellipsoidal fluorescence profile. Because we observe single QDs on the membrane surface and inside cells at early phases of endocytosis, this suggests that QD probes that we track are bound to single or small numbers of NGF-receptor dimmers, with little exception. These estimates are supported by recent ratiometric fluorescent intensity and TEM measurements of vesicle endosomes of QD-NGF treated primary DRG neurons.[38]

QD-NGF Treatment of PC12 Cells. PC12 cells (ATCC) were grown in collagen-coated T-75 flasks in RPMI-1640 (ATCC) supplemented with 10% horse serum (ATCC) and 5% fetal bovine serum (Gibco) at 37 °C. Upon reaching confluence, cells were trypsinized and replated at a density of 16 × 10^5 cells/mL onto poly-L-lysine coated glass-bottom Petri dishes (MatTek Corp) that were coated with 50 μg/ml collagen (rat tail type I, BD Biosciences). Unless otherwise noted, PC12 cells were incubated with NGF (β-NGF, 100 ng/ml) and allowed to differentiate for 2 days before performing experiments. For QD-NGF treatment, PC12 cells were rinsed gently with DMEM and incubated with 10 nM QD-NGF in DMEM for 15 min at 37 °C. Next, cells were gently rinsed twice with DMEM to remove unbound QD-NGFs, followed by cell media replacement with RPMI. Cells were then immediately placed on the microscope stage and imaged at room temperature at time durations from t = 0 to 150 min after QD-NGF treatment. Warmed RPMI media was exchanged during the imaging process to maintain adequate temperature. We found that under these imaging conditions, the rate of QD-NGF internalization, time course of QD-NGF migration toward the center of the cells, and fusion of multiple QD-NGF complexes into common endosomal compartments were similar to that of control experiments where QD-NGF treated cells were left in the incubator for extended durations (t = 45 and 90 min) before imaging.

QD-NGF Live Cell Image Acquisition. Images were acquired using a Zeiss Axiovert microscope equipped with a 100× objective and a cooled monochrome CCD camera (Axiocam). QD fluorescence was detected using excitation and emission filters (e460spuv, D655, Chroma). All time lapse videos were recorded at an overall frame interval of 79 ms (with the exception of two videos which had an overall frame interval of 110 ms) with a camera binning of 2 × 2 pixels. Image acquisition was done using AxioVision 4.4 Software (Zeiss).

Single QD Detection and Tracking. To quantify the average number of QDs per cell from static images, QD particle counts were made from fluorescence images using a dynamic segmentation filter (AutoMeasure Plus module in AxioVision, Zeiss). The reliability of these automated QD particle counts was verified by manual counting of the same images. To study the movement of single QD-NGF complexes, we used performed single particle tracking using the Image J Particle Tracker Plugin developed by I. F. Sbalzarini and P. Koumoutsakos.[84] For each video clip, individual QD-NGF complexes were detected by adjusting parameters for radius, cutoff, and percentile, as well as displacement, to maximize capture of the greatest number of QD-NGFs and ensure that the same QD-NGF complex was tracked in all video frames. A link range parameter of 3−4 frames (the number of consecutive frames over which interpolation occurs) was determined to successfully interpolate between frames in which QDs blink or momentarily disappear from the plane of focus (z-plane). All individual trajectories were visually inspected and only trajectories were further analyzed in which it was clear that the position of the same QD-NGF complex was extracted over the entire duration of observation. Individual trajectories for each QD were obtained as avi and text files, and analyzed using custom-written MATLAB (Mathworks, Inc.) programs.

Analysis of QD-NGF Trajectories. QD-NGF complexes undergoing active transport exhibited rapid, steplike displacements in position that did not return to the baseline, and traversed a net distance (see for example, Figure 5A). To quantify the magnitude and duration of QD-NGF displacements, or "run lengths", we used a moving average detection algorithm published by Watanabe *et al.*[29] A difference filter, diff, computed a moving average difference using the following formula:

$$\text{diff} = \frac{1}{m}\sum_{i=n+1}^{n+m} x_i - \frac{1}{m}\sum_{i=n-m}^{n-1} x_i \quad (1)$$

where x_n indicates the position of the nth point, and m is the size of the filter. The output of diff (Figure 5A, blue trace) represents the difference of mean positions over m data points before the nth point, from the mean positions over m data points after the nth point. To detect the occurrence of a run length, an std threshold filter was applied to the output of diff. Std threshold consisted of a moving filter which computes the standard deviation of m data points before and after the nth point and detects a run length if diff $>$ 3std. Both diff and std threshold were optimized so that the magnitude and duration of the run lengths were best preserved ($m = 9$) and so that all sustained excursions were detected as run lengths (thresholding criterion is diff $>$ 3std). A final thresholding filter, run length, using the criterion std threshold $>$ 0.6 μm, was applied to minimize false positives that were contributed by diffusive displacements (Figure 5A, orange arrow). The false positives were infrequent; visual inspection showed that of all detected 72 run-length events, only 4 resembled diffusive fluctuations. We verified that this final thresholding criterion, while minimizing false positives, did not overlook run lengths of lesser amplitude. Visual inspection showed that to minimize false positives, 14% of run lengths (11 of 79 total) were missed; however, these smaller run lengths had amplitudes that were close to threshold values (0.5 μm ± 0.096) and would not have appreciably changed the resulting amplitude histogram.

Immuno-colocalization of QD-NGFs and Endosomes. Differentiated PC12 cells were treated with 40 nM QD-NGFs for 15 min and then fixed with 4% paraformaldehyde at time points t = 15, 30, 45, 90, and 150 min and 12 h, after removal of unbound QD-NGFs. PC12 cells were then permeabilized with 0.25% Triton X-100 (15 mins), blocked with 10% normal horse serum (1 h) and incubated with primary antibodies: anti-EEA1 (5 μg/ml, Transduction Laboratories, KY) or anti-LAMP1 (5 μg/ml, Developmental Studies Hybridoma Databank, Iowa). Alexa 488-labeled goat antimouse IgG (5 μg/ml, Molecular Probes, OR) was used as the secondary antibody. Fluorescence images were obtained as serial optical sections (0.5 μm thickness) using an Apotome Unit (Zeiss).

QD Hybrid Gel Coimmunoprecipitation. To determine the association of TrkA receptors with QD-NGFs, we used a QD in-gel pull down technique we developed[18] to obtain electrophoretic blots of cell-internalized QD-NGFs, followed by hybridization with anti-TrkA antibody (C-14, Santa Cruz). Electrophoresis was performed at 90−150 V for 1−2 h with 1× TBE running buffer under native conditions using PA-AGE gels composed of a mixture of acrylamide−agarose (2% PA−0.5% AGE). PC12 cells were treated with 40 nM QD-NGFs for 15 min, washed, and then treated with lysis buffer (PBS, 10% glycerol and 0.25% NP-40) supplemented with protease inhibitor cocktail (Sigma) and phosphatase inhibitors (2 mM sodium orthovanadate and 10 mM sodium fluoride), at t = 0, 30, 90, 150 min after washing. Cell lysates were cleared and then mixed with loading buffer (40% w/v sucrose, 0.25% w/v bromophenol blue) and loaded at on hybrid PA-AGE gels. Protein concentration of the cell lysates were measured using the Bio-Rad Protein Assay and loaded at equal amounts (80 μg) into wells. Gel-fractionated QD-NGF complexes were transferred to PVDF membranes by electrophoretic blotting. PVDF membranes blots were hybridized with biotinylated anti-TrkA antibody. Antibody biotinylation was performed by incubation with 500-fold excess of NHS-PEO_4-biotin (Pierce) and followed by dialysis (slide-A-lyzer, 7KD MWCO, Pierce) against PBS (pH 7.2) to remove unbound biotin. PVDF membranes were blocked with 3% BSA and 0.8 μM avidin (Sigma) and subsequently hybridized with the biotinylated-anti-TrkA antibody (4 μg/ml in 1× TBS/ 0.1% Tween-20). Subsequently, membranes were washed (three times for 10 min each with 1× TBS/0.1% Tween-20) and streptavidin-525 QDs (green) was added (30 nM in blotting buffer) at 4 °C overnight. A final washing step was performed (1× TBS/0.1% Tween-20). Images of protein-QD blotted PVDF membranes were captured with a color digital camera under UV transillumination (UVP). Care was taken to capture and process pre- and posthybridization images under the same conditions. Images were transformed to RGB format and color channels were separated with equal weights using Image J.

Acknowledgment. We thank A. Ardeshiri for assistance with quantitative analysis and S. Cardin for comments on a draft of this manuscript. This work was supported by funding from DOD W81XWH-07-2-0107, Oregon ETIC, and the Oregon Medical Research Foundation (T.Q.V.).

Supporting Information Available: Figures S1 and S2. This material is available free of charge *via* the Internet at http://pubs.acs.org.

REFERENCES AND NOTES

1. Mukherjee, S.; Ghosh, R. N.; Maxfield, F. R. Endocytosis. *Physiol. Rev.* **1997**, *77* (3), 759–803.
2. Luby-Phelps, K. Physical Properties of Cytoplasm. *Curr. Opin. Cell. Biol.* **1994**, *6* (1), 3–9.
3. Luby-Phelps, K. Cytoarchitecture and Physical Properties of Cytoplasm: Volume, Viscosity, Diffusion, Intracellular Surface Area. *Int. Rev. Cytol.* **2000**, *192*, 189–221.
4. Gruenberg, J.; Maxfield, F. R. Membrane Transport in the Endocytic Pathway. *Curr. Opin. Cell. Biol.* **1995**, *7* (4), 552–63.
5. Smith, A. M.; Ruan, G.; Rhyner, M. N.; Nie, S. Engineering Luminescent Quantum Dots for in Vivo Molecular and Cellular Imaging. *Ann. Biomed. Eng.* **2006**, *34*, 3–14.
6. Chan, W. C.; Nie, S. Quantum Dot Bioconjugates for Ultrasensitive Nonisotopic Detection. *Science* **1998**, *281*, 2016–8.
7. Grecco, H. E.; Lidke, K. A.; Heintzmann, R.; Lidke, D. S.; Spagnuolo, C.; Martinez, O. E.; Jares-Erijman, E. A.; Jovin, T. M. Ensemble and Single Particle Photophysical Properties (Two-Photon Excitation, Anisotropy, Fret, Lifetime, Spectral Conversion) of Commercial Quantum Dots in Solution and in Live Cells. *Microsc. Res. Tech.* **2004**, *65*, 169–79.
8. Bruchez, M., Jr.; Moronne, M.; Gin, P.; Weiss, S.; Alivisatos, A. P. Semiconductor Nanocrystals as Fluorescent Biological Labels. *Science* **1998**, *281*, 2013–6.
9. Michalet, X.; Pinaud, F. F.; Bentolila, L. A.; Tsay, J. M.; Doose, S.; Li, J. J.; Sundaresan, G.; Wu, A. M.; Gambhir, S. S.; Weiss, S. Quantum Dots for Live Cells, *in Vivo* Imaging, and Diagnostics. *Science* **2005**, *307*, 538–44.
10. Alivisatos, A. P.; Gu, W.; Larabell, C. Quantum Dots as Cellular Probes. *Annual Review of Biomedical Engineering* **2005**, *7*, 55–76; three plates.
11. Rosenthal, S. J.; Tomlinson, I.; Adkins, E. M.; Schroeter, S.; Adams, S.; Swafford, L.; McBride, J.; Wang, Y.; DeFelice, L. J.; Blakely, R. D. Targeting Cell Surface Receptors with Ligand-Conjugated Nanocrystals. *J. Am. Chem. Soc.* **2002**, *124*, 4586–94.
12. Dahan, M.; Levi, S.; Luccardini, C.; Rostaing, P.; Riveau, B.; Triller, A. Diffusion Dynamics of Glycine Receptors Revealed by Single-Quantum Dot Tracking. *Science* **2003**, *302*, 442–5.
13. Lidke, D. S.; Nagy, P.; Heintzmann, R.; Arndt-Jovin, D. J.; Post, J. N.; Grecco, H. E.; Jares-Erijman, E. A.; Jovin, T. M. Quantum Dot Ligands Provide New Insights into Erbb/Her Receptor-Mediated Signal Transduction. *Nat. Biotechnol.* **2004**, *22*, 198–203.
14. Vu, T. Q.; Maddipati, R.; Blute, T. A.; Nehilla, B. J.; Nusblat, L; Desai, T. A. Peptide-Conjugated Quantum Dots Activate Neuronal Receptors and Initiate Downstream Signaling of Neurite Growth. *Nano Lett.* **2005**, *25*, 603–7.
15. Howarth, M.; Takao, K.; Hayashi, Y.; Ting., A. Y. Targeting Quantum Dots to Surface Proteins in Living Cells with Biotin Ligase. *Proc. Natl. Acad. Sci. U.S.A.* **2005**, *2102*, 7583–8.
16. Triller, A.; Choquet, D. Surface Trafficking of Receptors between Synaptic and Extrasynaptic Membranes: And yet They Do Move. *Trends Neurosci.* **2005**, *28*, 133–9.

17. Haggie, P. M.; Kim, J. K.; Lukacs, G. L.; Verkman, A. S. Tracking of Quantum Dot-Labeled Cftr Shows near Immobilization by C-Terminal Pdz Interactions. *Mol. Biol. Cell* **2006**, *17*, 4937–45.
18. Gussin, H. A.; Tomlinson, I. D.; Little, D. M.; Warnement, M. R.; Qian, H.; Rosenthal, S. J.; Pepperberg, D. R. Binding of Muscimol-Conjugated Quantum Dots to Gaba(C) Receptors. *J. Am. Chem. Soc.* **2006**, *128*, 15701–13.
19. Yu, G.; Liang, J.; He, Z.; Sun, M. Quantum Dot-Mediated Detection of Gamma-Aminobutyric Acid Binding Sites on the Surface of Living Pollen Protoplasts in Tobacco. *Chem Biol* **2006**, *13*, 723–31.
20. Bouzigues, C.; Morel, M.; Triller, A.; Dahan, M. Asymmetric Redistribution of Gaba Receptors During Gaba Gradient Sensing by Nerve Growth Cones Analyzed by Single Quantum Dot Imaging*Proc. Natl. Acad. Sci. U.S.A.* **2007**, *104*, 11251−6.
21. Bats, C.; Groc, L.; Choquet, D. The Interaction between Stargazin and Psd-95 Regulates Ampa Receptor Surface Trafficking. *Neuron* **2007**, *53*, 719–34.
22. Jaiswal, J. K.; Mattoussi, H.; Mauro, J. M.; Simon, S. M. Long-Term Multiple Color Imaging of Live Cells Using Quantum Dot Bioconjugates. *Nat. Biotechnol.* **2003**, *21*, 47–51.
23. Silver, J.; Ou, W. Photoactivation of Quantum Dot Fluorescence Following Endocytosis. *Nano Lett.* **2005**, *5*, 1445–9.
24. Nan, X.; Sims, P. A.; Chen, P.; Xie, X. S. Observation of Individual Microtubule Motor Steps in Living Cells with Endocytosed Quantum Dots. *J. Phys. Chem. B: Condens. Matter Mater. Surf. Interfaces Biophys.* **2005**, *109*, 24220–4.
25. Gu, W.; Pellegrino, T.; Parak, W. J.; Boudreau, R.; Le Gros, M. A.; Gerion, D.; Alivisatos, A. P.; Larabell, C. A. Quantum-Dot-Based Cell Motility Assay. *Sci. STKE* **2005**, *2005*, plate 5.
26. Seleverstov, O.; Zabirnyk, O.; Zscharnack, M.; Bulavina, L.; Nowicki, M.; Heinrich, J. M.; Yezhelyev, M.; Emmrich, F.; O'Regan, R.; Bader, A. Quantum Dots for Human Mesenchymal Stem Cells Labeling. A Size-Dependent Autophagy Activation. *Nano Lett.* **2006**, *6*, 2826–32.
27. Sundara Rajan, S.; Vu, T. Q. Quantum Dots Monitor Trka Receptor Dynamics in the Interior of Neural Pc12 Cells. *Nano Lett.* **2006**, *6*, 2049–59.
28. Duan, H.; Nie, S. Cell-Penetrating Quantum Dots Based on Multivalent and Endosome-Disrupting Surface Coatings. *J. Am. Chem. Soc.* **2007**, *129*, 3333–8.
29. Watanabe, T. M.; Higuchi, H. Stepwise Movements in Vesicle Transport of Her2 by Motor Proteins in Living Cells. *Biophys. J.* **2007**, *92*, 4109–20.
30. Cambi, A.; Lidke, D. S.; Arndt-Jovin, D. J.; Figdor, C. G.; Jovin, T. M. Ligand-Conjugated Quantum Dots Monitor Antigen Uptake and Processing by Dendritic Cells. *Nano Lett.* **2007**, *7*, 970–7.
31. Ruan, G.; Agrawal, A.; Marcus, A. I.; Nie, S. Imaging and Tracking of Tat Peptide-Conjugated Quantum Dots in Living Cells: New Insights into Nanoparticle Uptake, Intracellular Transport, and Vesicle Shedding. *J. Am. Chem. Soc.* **2007**, *129*, 14759–66.
32. Zweifel, L. S.; Kuruvilla, R.; Ginty, D. D. Functions and Mechanisms of Retrograde Neurotrophin Signalling. *Nat. Rev. Neurosci.* **2005**, *6*, 615–25.
33. Miaczynska, M.; Pelkmans, L.; Zerial, M. Not Just a Sink: Endosomes in Control of Signal Transduction. *Curr. Opin. Cell. Biol.* **2004**, *16*, 400–6.
34. Neet, K. E.; Campenot, R. B. Receptor Binding, Internalization, and Retrograde Transport of Neurotrophic Factors. *Cell. Mol. Life Sci.* **2001**, *58*, 1021–35.
35. Howe, C. L. Modeling the Signaling Endosome Hypothesis: Why a Drive to the Nucleus Is Better Than a (Random) Walk. *Theor. Biol. Med. Model* **2005**, *2*, 43.
36. von Zastrow, M.; Sorkin, A. Signaling on the Endocytic Pathway. *Curr. Opin. Cell Biol.* **2007**, *19*, 436–45.
37. Vu, T. Q.; Maddipati, R.; Blute, T. A.; Nehilla, B. J.; Nusblat, L.; Desai., T. A. Peptide-Conjugated Quantum Dots Activate Neuronal Receptors and Initiate Downstream Signaling of Neurite Growth. *Nano Lett.* **2005**, *5*, 603–7.
38. Cui, B.; Wu, C.; Chen, L.; Ramirez, A.; Bearer, E. L.; Li, W. P.; Mobley, W. C.; Chu, S. One at a Time, Live Tracking of Ngf Axonal Transport Using Quantum Dots. *Proc. Natl. Acad. Sci. U.S.A.* **2007**, *104*, 13666–71.
39. Echarte, M. M.; Bruno, L.; Arndt-Jovin, D. J.; Jovin, T. M.; Pietrasanta, L. I. Quantitative Single Particle Tracking of Ngf-Receptor Complexes: Transport Is Bidirectional but Biased by Longer Retrograde Run Lengths. *FEBS Lett.* **2007**, *581*, 2905–13.
40. Liu, H. Y.; Vu, T. Q. Identification of Quantum Dot Bioconjugates and Cellular Protein Co-Localization by Hybrid Gel Blotting. *Nano Lett.* **2007**, *7*, 1044–9.
41. Grimes, M. L.; Zhou, J.; Beattie, E. C.; Yuen, E. C.; Hall, D. E.; Valletta, J. S.; Topp, K. S.; LaVail, J. H.; Bunnett, N. W.; Mobley, W. C. Endocytosis of Activated Trka: Evidence That Nerve Growth Factor Induces Formation of Signaling Endosomes. *J. Neurosci.* **1996**, *16*, 7950–64.
42. Bernd, P.; Greene, L. A. Electron Microscopic Radioautographic Localization of Iodinated Nerve Growth Factor Bound to and Internalized by Pc12 Cells. *J. Neurosci.* **1983**, *3*, 631–43.
43. Jullien, J.; Guili, V.; Reichardt, L. F.; Rudkin, B. B. Molecular Kinetics of Nerve Growth Factor Receptor Trafficking and Activation. *J. Biol. Chem.* **2002**, *277*, 38700–8.
44. Bronfman, F. C.; Tcherpakov, M.; Jovin, T. M.; Fainzilber, M. Ligand-Induced Internalization of the P75 Neurotrophin Receptor: A Slow Route to the Signaling Endosome. *J. Neurosci.* **2003**, *23*, 3209–20.
45. Saxena, S.; Howe, C. L.; Cosgaya, J. M.; Steiner, P.; Hirling, H.; Chan, J. R.; Weis, J.; Kruttgen, A. Differential Endocytic Sorting of P75ntr and Trka in Response to Ngf: A Role for Late Endosomes in Trka Trafficking. *Mol. Cell. Neurosci.* **2005**, *28*, 571–87.
46. Tsui-Pierchala, B. A.; Ginty, D. D. Characterization of an Ngf-P-Trka Retrograde-Signaling Complex and Age-Dependent Regulation of Trka Phosphorylation in Sympathetic Neurons. *J. Neurosci.* **1999**, *19*, 8207–18.
47. Bhattacharyya, A.; Watson, F. L.; Pomeroy, S. L.; Zhang, Y. Z.; Stiles, C. D.; Segal, R. A. High-Resolution Imaging Demonstrates Dynein-Based Vesicular Transport of Activated Trk Receptors. *J. Neurobiol.* **2002**, *51*, 302–12.
48. Heerssen, H. M.; Pazyra, M. F.; Segal, R. A. Dynein Motors Transport Activated Trks to Promote Survival of Target-Dependent Neurons. *Nat. Neurosci.* **2004**, *7*, 596–604.
49. Riccio, A.; Pierchala, B. A.; Ciarallo, C. L.; Ginty, D. D. An Ngf-Trka-Mediated Retrograde Signal to Transcription Factor Creb in Sympathetic Neurons. *Science* **1997**, *277*, 1097–100.
50. Jullien, J.; Guili, V.; Derrington, E. A.; Darlix, J. L.; Reichardt, L. F.; Rudkin, B. B. Trafficking of Trka-Green Fluorescent Protein Chimerae During Nerve Growth Factor-Induced Differentiation. *J. Biol. Chem.* **2003**, *278*, 8706–16.
51. Butowt, R.; von Bartheld, C. S. Sorting of Internalized Neurotrophins into an Endocytic Transcytosis Pathway Via the Golgi System: Ultrastructural Analysis in Retinal Ganglion Cells. *J. Neurosci.* **2001**, *21*, 8915–30.
52. Zapf-Colby, A.; Olefsky, J. M. Nerve Growth Factor Processing and Trafficking Events Following Trka-Mediated Endocytosis. *Endocrinology* **1998**, *139*, 3232–40.
53. Delcroix, J. D.; Valletta, J. S.; Wu, C.; Hunt, S. J.; Kowal, A. S.; Mobley, W. C. Ngf Signaling in Sensory Neurons: Evidence That Early Endosomes Carry Ngf Retrograde Signals. *Neuron* **2003**, *39*, 69–84.
54. Gruenberg, J.; van der Goot, F. G. Mechanisms of Pathogen Entry through the Endosomal Compartments. *Nat. Rev. Mol. Cell Biol.* **2006**, *7*, 495–504.
55. Bernd, P.; Greene, L. A. Association of 125i-Nerve Growth Factor with Pc12 Pheochromocytoma Cells. Evidence for Internalization Via High-Affinity Receptors Only and for Long-Term Regulation by Nerve Growth Factor of Both High- and Low-Affinity Receptors. *J. Biol. Chem.* **1984**, *259*, 15509–16.
56. Gruenberg, J.; Griffiths, G.; Howell, K. E. Characterization of the Early Endosome and Putative Endocytic Carrier

Vesicles in Vivo and with an Assay of Vesicle Fusion in Vitro. *J. Cell Biol.* **1989**, *108*, 1301–16.
57. Nielsen, E.; Severin, F.; Backer, J. M.; Hyman, A. A.; Zerial, M. Rab5 Regulates Motility of Early Endosomes on Microtubules. *Nat. Cell Biol.* **1999**, *1*, 376–82.
58. de Bruin, K.; Ruthardt, N.; von Gersdorff, K.; Bausinger, R.; Wagner, E.; Ogris, M.; Brauchle, C. Cellular Dynamics of Egf Receptor-Targeted Synthetic Viruses. *Mol. Ther.* **2007**, *15*, 1297–305.
59. de Wit, H.; Lichtenstein, Y.; Geuze, H. J.; Kelly, R. B.; van der Sluijs, P.; Klumperman, J. Synaptic Vesicles Form by Budding from Tubular Extensions of Sorting Endosomes in Pc12 Cells. *Mol. Biol. Cell* **1999**, *10*, 4163–76.
60. Kholodenko, B. N. Four-Dimensional Organization of Protein Kinase Signaling Cascades: The Roles of Diffusion, Endocytosis and Molecular Motors. *J. Exp. Biol.* **2003**, *206*, 2073–82.
61. Mallik, R.; Gross, S. P. Molecular Motors: Strategies to Get Along. *Curr. Biol.* **2004**, *14*, R971–82.
62. Goldstein, L. S.; Yang, Z. Microtubule-Based Transport Systems in Neurons: The Roles of Kinesins and Dyneins. *Annu. Rev. Neurosci.* **2000**, *23*, 39–71.
63. Block, S. M.; Goldstein, L. S.; Schnapp, B. J. Bead Movement by Single Kinesin Molecules Studied with Optical Tweezers. *Nature* **1990**, *348*, 348–52.
64. Caspi, A.; Granek, R.; Elbaum, M. Diffusion and Directed Motion in Cellular Transport. *Phys. Rev. E Stat. Nonlin. Soft Matter Phys.* **2002**, *66*, 011916.
65. Courty, S.; Luccardini, C.; Bellaiche, Y.; Cappello, G.; Dahan, M. Tracking Individual Kinesin Motors in Living Cells Using Single Quantum-Dot Imaging. *Nano Lett.* **2006**, *6*, 1491–5.
66. Wang, Z.; Khan, S.; Sheetz, M. P. Single Cytoplasmic Dynein Molecule Movements: Characterization and Comparison with Kinesin. *Biophys. J.* **1995**, *69*, 2011–23.
67. Claude, P.; Hawrot, E.; Dunis, D. A.; Campenot, R. B. Binding, Internalization, and Retrograde Transport of 125i-Nerve Growth Factor in Cultured Rat Sympathetic Neurons. *J. Neurosci.* **1982**, *2*, 431–42.
68. Hirashima, N.; Nishio, M.; Nakanishi, M. Intracelluar Dynamics of a High Affinity Ngf Receptor Trka in Pc12 Cell. *Biol. Pharm. Bull.* **2000**, *23*, 1097–9.
69. Lidke, D. S.; Lidke, K. A.; Rieger, B.; Jovin, T. M.; Arndt-Jovin, D. J. Reaching out for Signals: Filopodia Sense Egf and Respond by Directed Retrograde Transport of Activated Receptors. *J. Cell Biol.* **2005**, *170*, 619–26.
70. Arhel, N.; Genovesio, A.; Kim, K. A.; Miko, S.; Perret, E.; Olivo-Marin, J. C.; Shorte, S.; Charneau, P. Quantitative Four-Dimensional Tracking of Cytoplasmic and Nuclear Hiv-1 Complexes. *Nat. Methods* **2006**, *3*, 817–24.
71. Mellman, I. Endocytosis and Molecular Sorting. *Annu. Rev. Cell Dev. Biol.* **1996**, *12*, 575–625.
72. von Bartheld, C. S. Axonal Transport and Neuronal Transcytosis of Trophic Factors, Tracers, and Pathogens. *J. Neurobiol.* **2004**, *58*, 295–314.
73. Brandenburg, B.; Zhuang, X. Virus Trafficking—Learning from Single-Virus Tracking. *Nat. Rev. Microbiol.* **2007**, *5*, 197–208.
74. Douglas, K. L.; Piccirillo, C. A.; Tabrizian, M. Cell Line-Dependent Internalization Pathways and Intracellular Trafficking Determine Transfection Efficiency of Nanoparticle Vectors. *Eur. J. Pharm. Biopharm.* **2008**, *68*, 676–87.
75. Lai, S. K.; Hida, K.; Man, S. T.; Chen, C.; Machamer, C.; Schroer, T. A.; Hanes, J. Privileged Delivery of Polymer Nanoparticles to the Perinuclear Region of Live Cells *via* a Non-Clathrin, Non-Degradative Pathway. *Biomaterials* **2007**, *28*, 2876–84.
76. Harush-Frenkel, O.; Debotton, N.; Benita, S.; Altschuler, Y. Targeting of Nanoparticles to the Clathrin-Mediated Endocytic Pathway. *Biochem. Biophys. Res. Commun.* **2007**, *353*, 26–32.
77. Nabiev, I.; Mitchell, S.; Davies, A.; Williams, Y.; Kelleher, D.; Moore, R.; Gun'ko, Y. K.; Byrne, S.; Rakovich, Y. P.; Donegan, J. F.; Sukhanova, A.; Conroy, J.; Cottell, D.; Gaponik, N.; Rogach, A.; Volkov, Y. Nonfunctionalized Nanocrystals Can Exploit a Cell's Active Transport Machinery Delivering Them to Specific Nuclear and Cytoplasmic Compartments. *Nano Lett.* **2007**, *7*, 3452–61.
78. Chung, T. H.; Wu, S. H.; Yao, M.; Lu, C. W.; Lin, Y. S.; Hung, Y.; Mou, C. Y.; Chen, Y. C.; Huang, D. M. The Effect of Surface Charge on the Uptake and Biological Function of Mesoporous Silica Nanoparticles in 3t3-L1 Cells and Human Mesenchymal Stem Cells. *Biomaterials* **2007**, *28*, 2959–66.
79. Suh, J.; Dawson, M.; Hanes, J. Real-Time Multiple-Particle Tracking: Applications to Drug and Gene Delivery. *Adv. Drug Delivery Rev.* **2005**, *57*, 63–78.
80. Lai, S. K.; Hida, K.; Chen, C.; Hanes, J. Characterization of the Intracellular Dynamics of a Non-Degradative Pathway Accessed by Polymer Nanoparticles. *J. Controlled Release* **2008**, *125*, 107–11.
81. Thorn, K. S.; Ubersax, J. A.; Vale, R. D. Engineering the Processive Run Length of the Kinesin Motor. *J. Cell Biol.* **2000**, *151*, 1093–100.
82. Nehilla, B. J.; Vu, T. Q.; Desai, T. A. Stoichiometry-Dependent Formation of Quantum Dot-Antibody Bioconjugates: A Complementary Atomic Force Microscopy and Agarose Gel Electrophoresis Study. *J. Phys. Chem. B: Condens. Matter Mater. Surf. Interfaces Biophys.* **2005**, *109*, 20724–30.
83. Pattani, V. P.; Li, C.; Desai, T. A.; Vu, T. Q. Microcontact Printing of Quantum Dot Bioconjugate Arrays for Localized Capture and Detection of Biomolecules. *Biomed. Microdevices* **2008**, *10*, 367–74.
84. Sbalzarini, I. F.; Koumoutsakos, P. Feature Point Tracking and Trajectory Analysis for Video Imaging in Cell Biology. *J. Struct. Biol.* **2005**, *151*, 182–95.